WPPFC-PR(17) 17116

M Komm et al.

On thermionic emission from plasma-facing components in tokamak-relevant conditions

Preprint of Paper to be submitted for publication in
Plasma Physics and Controlled Fusion

This work has been carried out within the framework of the EUROfusion Consortium and has received funding from the Euratom research and training programme 2014-2018 under grant agreement No 633053. The views and opinions expressed herein do not necessarily reflect those of the European Commission.

This document is intended for publication in the open literature. It is made available on the clear understanding that it may not be further circulated and extracts or references may not be published prior to publication of the original when applicable, or without the consent of the Publications Officer, EUROfusion Programme Management Unit, Culham Science Centre, Abingdon, Oxon, OX14 3DB, UK or e-mail Publications.Officer@euro-fusion.org

Enquiries about Copyright and reproduction should be addressed to the Publications Officer, EUROfusion Programme Management Unit, Culham Science Centre, Abingdon, Oxon, OX14 3DB, UK or e-mail Publications.Officer@euro-fusion.org

The contents of this preprint and all other EUROfusion Preprints, Reports and Conference Papers are available to view online free at http://www.euro-fusionscipub.org. This site has full search facilities and e-mail alert options. In the JET specific papers the diagrams contained within the PDFs on this site are hyperlinked

On thermionic emission from plasma-facing components in tokamak-relevant conditions

M. Komm[1], S. Ratynskaia[2], P. Tolias[2], J. Cavalier[1], R. Dejarnac[1], J. P. Gunn[3] and A. Podolnik[1,4]

[1] Institute of Plasma Physics AS CR, v.v.i., Za Slovankou 3, 182 00 Prague 8, Czech Republic
[2] Space & Plasma Physics, KTH Royal Institute of Technology, 10044 Stockholm, Sweden
[3] CEA, IRFM, F-13108 Saint-Paul-lez-Durance, France
[4] MFF Charles University, V Holešovičkách 2, 180 00 Prague 8, Czech Republic

E-mail: komm@ipp.cas.cz

Abstract. The first results of Particle-In-Cell simulations of the electrostatic sheath and magnetic pre-sheath of thermionically emitting planar tungsten surfaces in fusion plasmas are presented. Plasma conditions relevant during edge localized modes (ELMs) and during inter-ELM periods have been considered for various inclinations of the magnetic field and selected surface temperatures. All runs have been performed under two assumptions for the sheath potential drop; fixed and floating. The primary focus lies on the quantification of the escaping thermionic current and the suppression factor due to the combined effects of space-charge and Larmor gyration. When applicable, the results are compared with the predictions of analytical models. The heat balance in the presence of thermionic emission as well as the contribution of the escaping thermionic current to surface cooling are also investigated. Regimes are identified where cooling due to emission has to be taken into account in the energy budget.

Submitted to: *Plasma Phys. Control. Fusion*

1. Introduction

The shaping of the tungsten monoblock front surface in high heat flux target areas is the key remaining physics design issue for the ITER divertor [1]. It has instigated coordinated cross-machine experiments [1–4], where specially designed plasma-facing components (PFCs) have successfully reached melting during exposure to stationary and transient plasma heat loads. At such elevated temperatures, the unimpeded thermionic current density, as described by the Richardson-Dushman formula, should exceed the incident plasma current densities by several orders of magnitude. It can, thus, be expected to have a strong impact not only on the melt layer dynamics [1] but also on the plasma boundary in local and even global scales. In particular: (i) thermionic emission could drive the macroscopic melt motion by triggering the replacement current responsible for the $\mathbf{J} \times \mathbf{B}$ force acting on the melt layer, (ii) the emitted electrons remove part of the PFC internal energy and could serve as an important cooling channel, (iii) the emitted electrons modify the sheath potential structure and could alter the incident plasma heat flux, (iv) the large ejected currents could lead to flux tube charging and consequent modification of transport in the divertor or scrape-off layer (SOL) regions.

It is evident that for the reliable calculation of the temperature excursions of PFC surfaces and the quantitative simulation of melt layer dynamics with codes such as MEMOS [5, 6], the escaping thermionic current density is a necessary input. The latter can be much lower than the nominal Richardson value due to two strongly entwined suppression mechanisms:

- **Space-charge effect.** For high emitted fluxes comparable to the plasma fluxes, locally accumulated electrons can reach a charge density that suffices to generate a potential minimum in the surface vicinity. The potential well (or virtual cathode) forces a fraction of the thermionic electrons to return to the surface. As a result, the escaping current is not only dictated by the surface temperature but also regulated by the space-charge. This is the so-called space-charge limited regime [7].
- **Prompt re-deposition.** In the presence of shallow magnetic fields, the low energy thermionic electrons can return to the PFC surface during their first gyration [8, 9]. The recapture probability also strongly depends on the local potential profile, since electric fields and electromagnetic drifts can either facilitate or inhibit prompt re-deposition.

There have been numerous theoretical descriptions of space-charge effects in the unmagnetized limit [10–13] and of prompt re-deposition for monotonic potential profiles [14–16]. However, they are not strictly valid for most fusion-relevant scenarios, where the grazing magnetic field incidence guarantees the importance of prompt re-deposition and the elevated PFC temperatures ensure that emission is strong enough for potential wells to form. For the applications of interest, the determination of the trajectories of the strongly magnetized thermionic electrons in the self-consistent non-monotonic electrostatic potential and of their possible intersection with the PFC surface is an analytically intractable problem. Nonetheless, Particle-In-Cell (PIC) simulations offer the possibility of treating thermionic suppression without oversimplifying assumptions. The necessity for PIC simulations becomes even more conspicuous when complex castellated geometries are considered [17].

Here we present the first results of PIC modelling of the electrostatic sheath and magnetic pre-sheath for thermionically emitting planar tungsten PFCs under tokamak-relevant plasma conditions. The 2D3V SPICE2 code has been employed [18, 19]. The runs were carried out for various inclinations of the magnetic field and selected surface temperatures. Two boundary conditions have been assumed; fixed potential drop and a potential drop satisfying the floating condition corresponding to no response and full response from the plasma, respectively. The primary focus lies on the quantification of the escaping thermionic current and the suppression factor due to the combined effects of the space-charge and Larmor gyration. When applicable, the results are compared with the predictions of analytical models. The effect of the potential structure on the impacting heat fluxes and the contribution of the escaping thermionic current to PFC cooling are also investigated.

2. Implementation of the problem in the SPICE2 code

SPICE2 is a 2D3V Cartesian PIC code, which calculates the motion of charged particles in a prescribed static magnetic field and a self-consistent electric field [18, 19]. The code is optimized for the simulation of particles in the electrostatic sheath and magnetic pre-sheath of PFCs oriented at oblique angles with respect to the magnetic field. For the purpose of this study, the code has been extended to include the generation of thermionic electrons and to incorporate some microphysical aspects of heat exchange with the PFC surface.

2.1. Modelling of thermionic emission and heat flux collection

The thermionic current density is described by the Richardson-Dushman formula [20]

$$j_{\rm th}^{\rm nom} = A_{\rm eff} T_{\rm s}^2 \exp\left(-\frac{W_{\rm f}}{kT_{\rm s}}\right), \tag{1}$$

where $T_{\rm s}$ is the surface temperature, $W_{\rm f}$ is the room temperature work function of the material, k is the Boltzmann constant and $A_{\rm eff}$ is the effective Richardson constant. Neglecting band theory effects in the density of states, quantum mechanical effects in electron transmission through the surface potential barrier and the nearly linear temperature dependence of the work function, one ends up with the nominal Richardson constant $A_0 = (4\pi m_{\rm e} e k^2)/h^3 \simeq 120\,{\rm Acm^{-2}K^{-2}}$ [20]. The effective Richardson constant incorporates these non-ideal effects and is generally lower than A_0 [21]. For atomically clean polycrystalline tungsten, reliable measurements have yielded $W_{\rm f} = 4.55\,{\rm eV}$ [22] and $A_{\rm eff} = 60\,{\rm Acm^{-2}K^{-2}}$ [23]. The v_x and v_y velocity components of the ejected electrons follow a Maxwellian distribution, whereas the v_z component follows a half-Maxwellian distribution ($\hat{\mathbf{z}}$ is chosen to coincide with the PFC surface normal). The temperature of these distributions is equal to $T_{\rm s}$ [20].

The routines responsible for the handling of the heat flux delivered to the PFC have been updated in the following manner: **(i)** When a thermionic electron is emitted, not only its kinetic energy is subtracted from the given point of the surface but also an energy equal to the work function, *i.e.* $E_{\rm th}^{\rm surf} = -(1/2)m_{\rm e}v^2 - W_{\rm f}$ [20]. The latter stems from the replacement electron that is pulled from the bulk to fill the thermal vacancy, thus driving a current through

the vessel. This replacement is assumed to take place at the Fermi level [24]. **(ii)** For each impinging electron, the total energy added to the intersection point with the PFC surface is given by $E_{\rm e}^{\rm surf} = (1/2)m_{\rm e}v^2 + W_{\rm f}$. The second term represents the additional heat generated during the equilibration of the absorbed electron at the top of the tungsten valence band. **(iii)** Concerning the collection of plasma ions, we have assumed a 100% accommodation and 100% neutralization probability. The former assumption was made in order to avoid the large uncertainties that characterize the reflection coefficients for low incident ion energies [25, 26], whereas the latter assumption is justified by the comparatively large interaction times and the valence electron availability for tunnelling [27]. For each absorbed ion, the total energy added to the intersection point is given by $E_{\rm i}^{\rm surf} = (1/2)m_{\rm i}v^2 + (U_{\rm iz} - W_{\rm f}) + U_{\rm sb}$, where $U_{\rm iz}$ is the ionization energy (13.6 eV for deuterium) and $U_{\rm sb}$ is the surface binding energy (1 eV for deuterium on tungsten [28]). The second term represents the total heat generated by potential energy release due to neutralization, while the third term represents the energy required to remove the ion from its local adsorption site [29].

The dependence of the thermionic current on the surface temperature implies a strong coupling between the plasma sheath properties and material heating. Since the simulation time is very short ($< 1\,\mu$s), it is not possible to monitor the self-consistent evolution of the surface temperature due to the impacting heat fluxes. Instead, a constant temperature $T_{\rm s}$ has been implemented for the whole PFC surface, leading to the stationary uniform emission of thermionic electrons. In the case of strong re-deposition of the thermionic electrons, the finiteness of the grid size and the time step lead to significant numerical errors on the heat fluxes deposited to the surface, since the termination point might not be equipotential with the ejection point. For this reason, the original energy at which each electron was ejected is stored in memory during the course of the simulation, and should this electron be reabsorbed, this exact energy is deposited to the PFC.

2.2. Simulation geometry and boundary conditions

A typical geometry for the SPICE2 simulation box is shown in Fig.1(a). The plasma particles are injected from the top boundary and propagate towards the PFC surface at the bottom. The side boundaries are periodic. The ions are injected into the simulation region with a parallel velocity distribution function given by a 1D quasineutral kinetic model of the scrape-off layer [30], while the electrons are Maxwellian. We note that due to the finite ion temperature, the $c_{\rm s} = \sqrt{(T_{\rm e} + T_{\rm i})/m_{\rm i}}$ definition of the Bohm speed is employed. The injection of plasma ions and electrons is fixed regardless of the presence of thermionic electrons. The possible violation of quasi-neutrality near the injection plane due to the escaping thermionic electrons is handled by source sheath formation, which self-consistently repels an adequate amount of plasma electrons and prevents them from entering the simulated area.

In Fig.1(b), the compression of the thermionic current for grazing magnetic field incidence is illustrated. The oblique angle between the PFC surfaces and the magnetic field allows the spreading of the incoming heat fluxes onto a large area. On the contrary, the thermionic current emitted from the surface is compressed by the magnetic field into a narrow

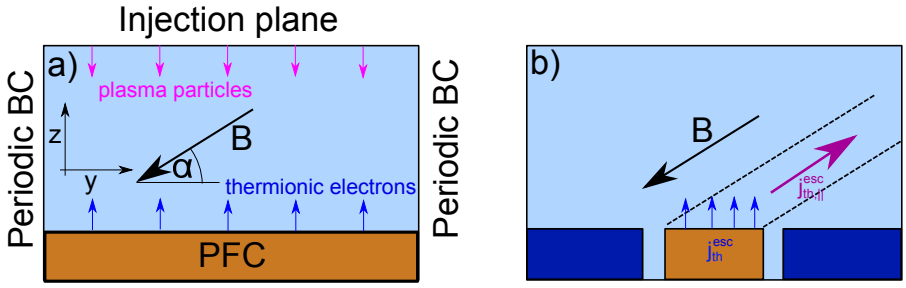

Figure 1. (a) Schematic of the SPICE2 simulation geometry. (b) Illustration of the compression of the escaping thermionic current density for grazing magnetic field incidence.

flux tube. This can further increase the already enormous emitted current density. If such a current were to be injected into the plasma, it could lead to modification of the scrape-off layer currents [31, 32] with subsequent effects on transport.

Tokamak PFCs are made of conducting materials which are typically electrically connected to the vessel (ground reference). This can lead to local violation of flux ambipolarity, meaning that the PFCs can receive non-zero current from the plasma [33] (which then closes through the vessel) and do not have to be electrically floating with respect to the local plasma potential. Due to the connection to the ground, even in the case of significant emitted current injected into the plasma, there is no change in the absolute value of the PFC potential. On the other hand, such injected current can lead to a modification of the local plasma potential [34], effectively changing the potential drop in the sheath. The magnitude of this response can vary depending on the plasma conditions not only in the vicinity of the PFC but possibly in the entire SOL. The determination of such a response is clearly outside the scope of this study. Instead, we will investigate two extreme cases: **(1)** the PFC-plasma potential difference is fixed at $-3T_\mathrm{e}/e$, which corresponds to no response from the plasma. In this case the incoming electron flux is always balanced by the ion flux only. **(2)** the PFC is floating, which corresponds to full response from the plasma. In this case, the potential is determined during the course of the simulation by minimizing the total incident current, thus the sheath potential drop is modified by emission in a manner that ensures ambipolarity.

2.3. Plasma parameters and scenarios

Results for both inter-ELM and intra-ELM plasmas are presented, but the primary focus lies on the former case. For inter-ELM conditions, parametric scans in the angle of incidence and surface temperature have been performed, whereas for ELM conditions few selected scenarios have been analyzed. The motivation behind such choice is manifold: (i) Transient melting occurs during ELMs, but the PFC remains at elevated temperatures for a longer time due to the finite thermal diffusivity. In other words, the characteristic heat diffusion time is longer than the ELM duration. To be more quantitative, 30 ms is a typical ELM cycle duration [2] in JET with the ELM lasting $1-3$ ms [40] and the typical intra-ELM PFC temperature rise being $\sim 100-300$ K (see for instance Fig.24 of Ref.[2]). (ii) The inter-ELM plasma heat fluxes are

much lower than those during ELMs, hence cooling due to thermionic emission can become significant. In a similar manner, the escaping thermionic currents during inter-ELM periods are more likely to play an important role in SOL transport. (iii) Accurate determination of the re-solidification instant during inter-ELM periods is a key aspect of macroscopic erosion [1, 5, 6], since it coincides with the arrest of melt-layer motion. (iv) Plasma conditions during inter-ELM periods are much better characterised than during ELMs, where measurements with an adequate temporal resolution are problematic due to the dramatic parameter evolution.

The following plasma conditions were chosen to reflect typical **inter-ELM** SOL and attached divertor conditions in contemporary machines: $T_\mathrm{i} = T_\mathrm{e} = 20\,\mathrm{eV}$, $n_\mathrm{e} = 10^{19}\,\mathrm{m}^{-3}$, $B = 3\,\mathrm{T}$ and deuterium plasma. The magnetic field inclination angle was varied between 5° and 90° with respect to the PFC normal, with the near-normal angles relevant for leading edge exposures. We shall study four different surface temperatures: $0\,\mathrm{K}$ (reference case with no emission), $2900\,\mathrm{K}$ (thermionic current of the order of the ion saturation current), $3400\,\mathrm{K}$ (characteristic re-solidification temperature at the inter-ELM period when ELMs lead to tungsten flash melting) and $3695\,\mathrm{K}$ (tungsten melting point). Note that for $T_\mathrm{e} = 20\,\mathrm{eV}$ electron induced electron emission is insignificant; secondary electron emission is negligible [35] and low energy quasi-elastic electron reflection is around 20% [36]. Electron reflection could play a role in the virtual cathode dynamics, since it concerns both the incident electrons and the redeposited thermionic electrons, but it will not be considered in this work.

For **intra-ELM** conditions, the plasma parameters employed are relevant to JET Type I ELMs. As a result of computational feasibility considerations, the scenario S3 from Ref.[37] has been chosen, which corresponds to $n_\mathrm{e} = 2 \times 10^{19}\,\mathrm{m}^{-3}$ and $T_\mathrm{e} = T_\mathrm{i} = 100\,\mathrm{eV}$. Three magnetic field orientations were simulated; perpendicular incidence (which corresponds to the plasma wetted side of the protruding lamella), $\alpha = 17.5^\circ$ incidence (surface of the sloped lamella) and grazing $\alpha = 5^\circ$ incidence (top surface of the lamellae). The actual angle of incidence on the top of the lamella ($\alpha = 2.5^\circ$) was not simulated due to computational limitations. All runs have been performed for $T_\mathrm{s} = 3695\,\mathrm{K}$. Even higher temperatures beyond the melting point would be relevant, but then the vaporization flux would become significant and would possibly affect particle and heat transport through the sheath, thus compromising the validity of our model and the accuracy of our results. Finally, we point out that for $T_\mathrm{e} = 100\,\mathrm{eV}$ electron induced electron emission is still not important [35].

The equality of the thermionic electron temperature with the PFC surface temperature results in a large ratio between the plasma and emitted electron temperatures. For instance, in the inter-ELM case we have $T_\mathrm{e}/kT_\mathrm{s} \sim 70$ even for $T_\mathrm{s} = 3400\,\mathrm{K}$ and in the intra-ELM case we have $T_\mathrm{e}/kT_\mathrm{s} \sim 300$ for $T_\mathrm{s} = 3695\,\mathrm{K}$. Moreover, since the virtual cathode is formed in order to suppress the emitted electrons, its magnitude should be of the order of kT_s/e. Numerical fluctuations present in the SPICE2 Poisson solver correspond to a very small fraction of T_e, which can be, however, equivalent to a sizeable fraction of kT_s. The above imply that numerical uncertainties set a rather stringent precision limit in the virtual cathode magnitude and thus also in the thermionic suppression factor.

The following definitions for the current densities are employed throughout the remaining text: $j_\mathrm{th}^\mathrm{nom}$ corresponds to the *nominal* unimpeded current density emitted according

to Eq.(1), $j_{\rm th}^{\rm esc}$ is the *escaping* thermionic current density (*i.e.* the current density which reaches the unperturbed plasma), $\eta_{\rm th} = j_{\rm th}^{\rm nom}/j_{\rm th}^{\rm esc}$ is the thermionic current suppression factor and $j_{\rm th,||}^{\rm esc} = j_{\rm th}^{\rm esc}/\sin\alpha$ is the parallel escaping current density, where α is the B-field inclination angle. We also point out that, in an effort to remain consistent with the nomenclatures of plasma and surface physics, the plasma temperatures are expressed in electron-volts but the surface and thermionic electron temperatures are expressed in Kelvin.

2.4. Determination of the mesh size

In the space-charge limited regime, a fine mesh must be employed to resolve the magnitude and position of the virtual cathode. Traditionally, PIC codes use cell sizes that are comparable to the plasma Debye length $\lambda_{\rm D}$ [38]. However, since the cold thermionic electrons that are responsible for the formation of the virtual cathode are characterized by a smaller Debye length, the potential well typically forms at distances much closer to the surface than $\lambda_{\rm D}$ [12] and the cell size has to be reduced. The potential profiles for different cell sizes d_z are presented in Fig.2; for (a) $\alpha = 90°$ and (b) $\alpha = 5°$, $T_{\rm s} = 3400\,{\rm K}$ and a fixed potential drop. We assume that the potential profile is well-resolved if the minimum appears farther than one cell above the surface (located at $z = 3\lambda_{\rm D}$ in this case). This is due to the fact that the electric field in SPICE2 is calculated as the finite difference of potentials between neighboring grid points, *i.e.* $E_z(z_i) = -[\phi(z_{i+1}) - \phi(z_{i-1})]/2d_z$. For $\alpha = 5°$, this condition is satisfied for $d_z = 0.1\lambda_{\rm D}$, but the well magnitude is matched even for coarser meshes. For $\alpha = 90°$, even for meshes as fine as $d_z = 0.025\lambda_{\rm D}$ the virtual cathode does not appear.

Fig.3 displays the variation of the particle fluxes as a function of the cell size d_z for (a) $\alpha = 90°$ and (b) $\alpha = 5°$, again for $T_{\rm s} = 3400\,{\rm K}$ and a fixed sheath potential drop.

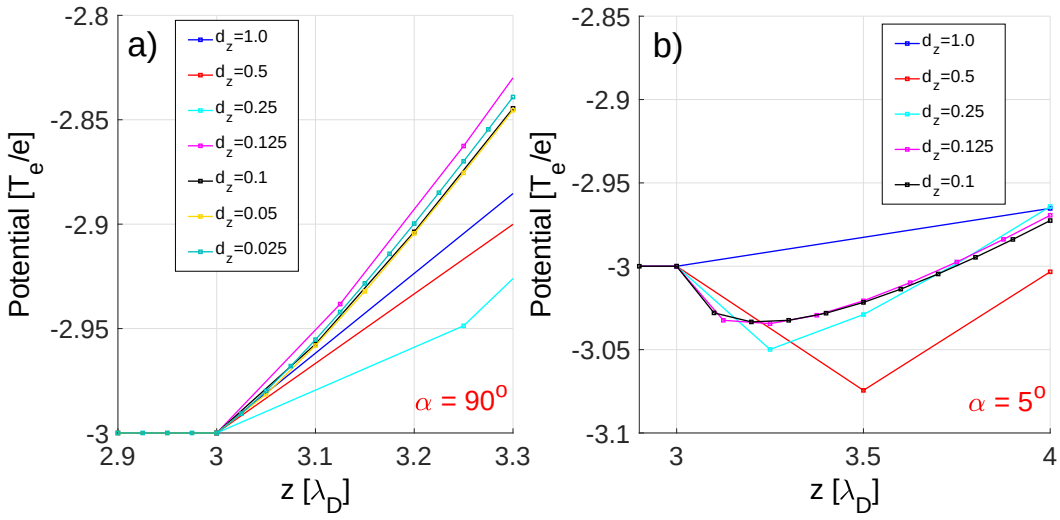

Figure 2. The potential profile in the vicinity of the PFC surface, under the assumption of a fixed sheath potential drop, for varying cell sizes $d_z/\lambda_{\rm D}$ and two magnetic field inclinations: (a) $\alpha = 90°$, (b) $\alpha = 5°$.

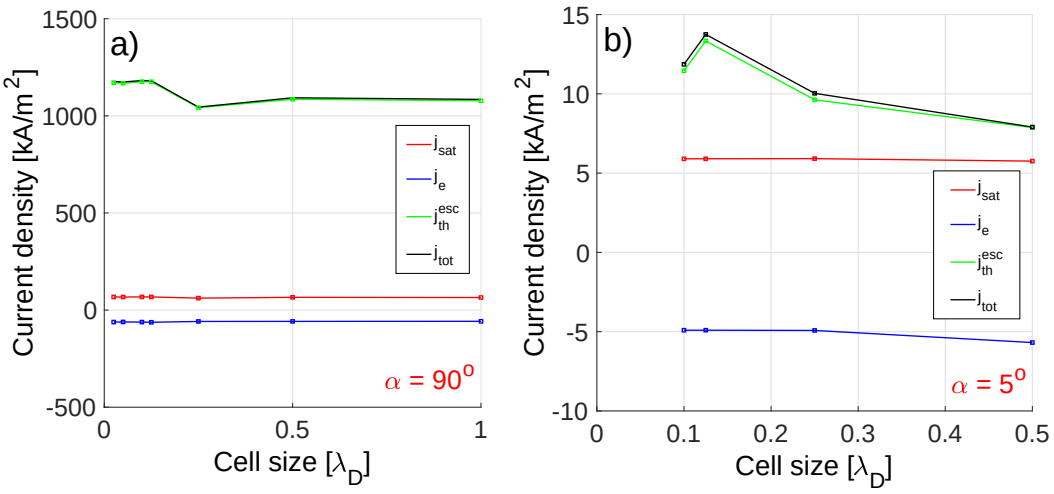

Figure 3. The current densities to the PFC surface, under the assumption of a fixed sheath potential drop, for varying cell sizes $d_z/\lambda_{\rm D}$ and two magnetic field inclinations: (a) $\alpha = 90°$, (b) $\alpha = 5°$.

In both cases, the values are essentially independent of d_z, which supports the validity of our simulations. Notice that for $\alpha = 5°$, the incoming particle fluxes are reduced due to the glancing angle of incidence and the escaping thermionic current is lower due to prompt re-deposition and virtual cathode formation. The virtual cathode depth is $\Phi_{\rm vc} = \phi_{\rm s} - \phi_{\rm vc} \sim 0.05 T_{\rm e}/e$ (normalized by the temperature of the plasma electrons) and corresponds to $\sim 3.4 k T_{\rm s}/e$ (normalized by the temperature of the thermionic electrons). This implies that small $\Phi_{\rm vc}$ variations caused by the insufficiently small grid size can cause considerable variations in the escaping current but not in the collected plasma current. In fact, after a comparison between Figs.2,3, it can be observed that the escaping current variations mirror the $\Phi_{\rm vc}$ variations. However, with an appropriate cell size d_z selection, such errors can always lie within 20% of the escaping current, which we consider to be an adequate precision limit. Overall, in order to properly resolve the virtual cathode for all the targeted scenarios, we will employ $d_z = 0.1\lambda_{\rm D}$ in the simulations that follow.

2.5. Role of surface roughness

The geometrical nature of prompt re-deposition suggests a dependance on surface roughness. Typical arithmetic mean roughness values for solid PFCs exceed one micrometer [39]. In the case of molten PFCs, melt layer motion that is driven by the $\mathbf{J} \times \mathbf{B}$ force, the plasma pressure or surface tension gradients leads to melt heights also in the micrometer range [1, 5]. Since the thermal Larmor radius of the thermionic electrons is $r_{\rm L,th} \leq 0.5\mu$m, the above imply that roughness can strongly influence thermionic suppression. Assuming a sinusoidal idealization of the plasma wetted surface, it is straightforward that electrons emitted from the crests will less likely be deposited by gyration, whereas electrons emitted from the troughs

will be characterized by increased prompt re-deposition. Therefore, in order to determine whether roughness enhances or mitigates thermionic suppression, an accurate mathematical model of the surface at the $r_{\mathrm{L,th}}$ scale is required.

Unless advanced body-fitted PIC approaches are followed which requires the introduction of mapping from a physical space (where the mesh conforms to the boundary) to a logical space domain (where the PIC algorithm is applied) [41], the shape of objects is approximated by cells of the cartesian PIC grid, which makes it impossible to simulate the realistic profile of a rough surface. Here, in order to acquire some qualitative results, emission from the crests has been mimicked by allowing the emission of electrons at distances d_{r} above the nominal surface plane. As expected, it has been observed that for $d_{\mathrm{r}} < r_{\mathrm{L,th}}$ prompt re-deposition still forces the thermionic electrons to return to the surface for shallow B-field angles, but for larger d_{r}, the virtual cathode becomes the dominant effect limiting the escaping current. Provided that $d_{\mathrm{r}} \leq 0.1\lambda_{\mathrm{D}}$, it has been concluded that the results are not sensitive to the exact value of d_{r}. In the simulations that follow, we have employed $d_{\mathrm{r}} = 0.0001\lambda_{\mathrm{D}}$, which essentially corresponds to a perfectly planar PFC.

3. Numerical results and comparison with theory

3.1. Results for inter-ELM plasma conditions

The results of a two-dimensional scan in the angle of incidence $\alpha = 5,\ 10,\ 20,\ 45,\ 90^{\circ}$ and the surface temperature $T_{\mathrm{s}} = 0,\ 2900,\ 3400, 3695\,\mathrm{K}$ - for both fixed and floating conditions - are presented in this section. In the following figures, the solid lines always represent results for a fixed sheath potential drop and the dashed lines for a floating surface.

The potential profile and the emergence of the virtual cathode close to the emitting surface are shown in the previous section. Here we focus on the depth of the virtual cathode - shown in Fig.4(a) - normalized to the surface temperature. Within our accuracy level, when $T_{\mathrm{s}} = 2900\,\mathrm{K}$, emission is not strong enough for the space-charge limited regime to be reached and the potential is still monotonic. This is also true when $T_{\mathrm{s}} = 3400\,\mathrm{K}$ and $\alpha = 90^{\circ}$, but only for the fixed potential drop condition and not for the floating condition. In all other cases, the potential well exists and is always deeper for the floating condition (for the same T_{s}, α). The potential well depth is of the order of one to a few kT_{s}/e with a clear increasing trend as the inclination angle decreases. This might appear as somewhat counterintuitive, since it could be argued that the enhanced suppression of emission due to the increased effectiveness of prompt re-deposition at shallower angles would suffice to prevent charge build-up and thus virtual cathode formation. However, simultaneously the small angle of incidence leads to the reduction of the plasma electron current density, increasing the ratio of the parallel escaping electron current density to the incoming electron current density, which can be confirmed by dividing the data presented in Fig.5(c) by $\sin\alpha$. In addition, the Larmor radius of the thermionic electrons is smaller but still comparable to the distance of the potential well from the surface, which clearly implies that even the electrons that are promptly re-deposited contribute to negative space-charge accumulation.

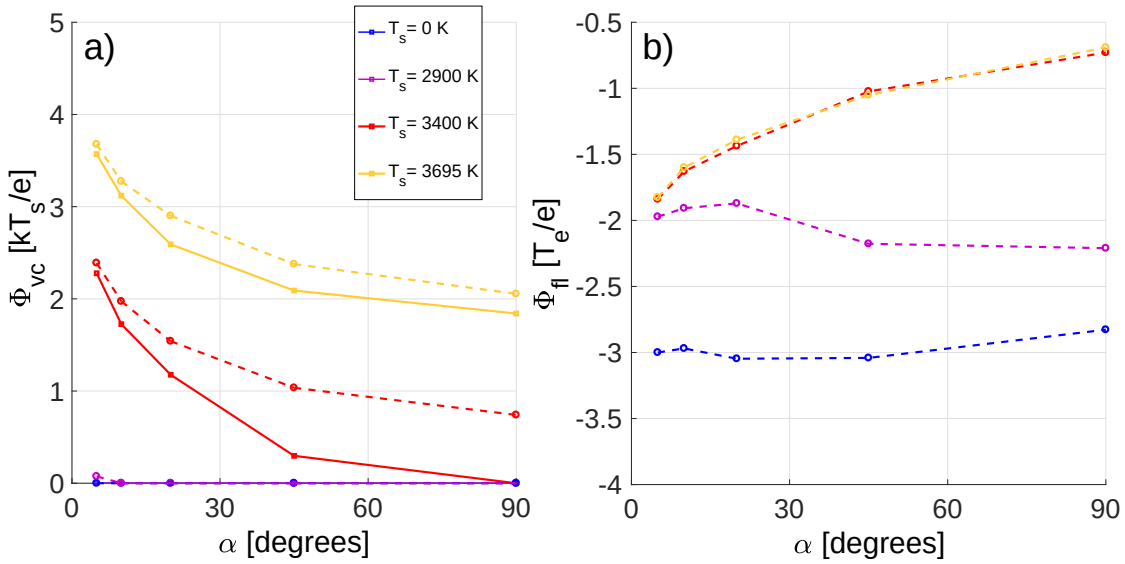

Figure 4. (a) The depth of the virtual cathode $\Phi_{\rm vc}$ in units of $kT_{\rm s}/e$ (for each temperature respectively) as a function of the inclination angle. (b) The floating potential $\Phi_{\rm fl}$ in units of $T_{\rm e}/e$ as a function of the inclination angle for different surface temperatures. The solid lines represent results for a fixed sheath potential drop and the dashed lines for a floating surface.

The floating potential (normalized to the electron temperature) as a function of the inclination angle is illustrated in Fig.4(b). Naturally, thermionic emission shifts the floating potential towards more positive values, thus the escaping thermionic current is compensated by an increased incident electron current as compared to the non-emitting case. The most positive values are reached for the least suppressed emission, which is realized at normal incidence. Despite the potential shift, the PFC surface always remains negative with respect to the plasma and an inverted sheath behavior is never observed. It is worth pointing out that the floating potential in absence of emission fluctuates around -3$T_{\rm e}/e$, these small deviations are indicative of the accuracy level of the PIC simulations.

The escaping thermionic currents are shown in Fig.5(a)-(d) in various normalizations. Fig.(a) presents $j_{\rm th}^{\rm esc}$ as a fraction of the nominal current given by the Richardson formula, *i.e.* the suppression factor $\eta_{\rm th}$. In absence of the virtual cathode, $T_{\rm s} = 2900\,$K, the surface emits 100% of the Richardson current for near-normal incidence. For inclinations of 20° and below, prompt re-deposition starts to be effective, providing an extra reduction in addition to the space-charge effect. In Fig.5(b) the parallel escaping current density $j_{\rm th,||}^{\rm esc} = j_{\rm th}^{\rm esc}/\sin\alpha$ is plotted in absolute magnitude. The values of the parallel escaping current density are high, from above $100\,$kA/m^2 at grazing angles up to $1\,$MA/m^2 at normal incidence. Finally, the escaping current is expressed as fraction of the incoming electron and ion fluxes - Figs.5(c,d) - in order to enable a straightforward comparison with the limiting cases described by analytical models, as we shall see in subsection 3.3.

In Fig.6(a), the cooling flux to the PFC due to the escaping thermionic electrons is compared with the heating flux to the PFC due to the incident plasma in an effort to address the

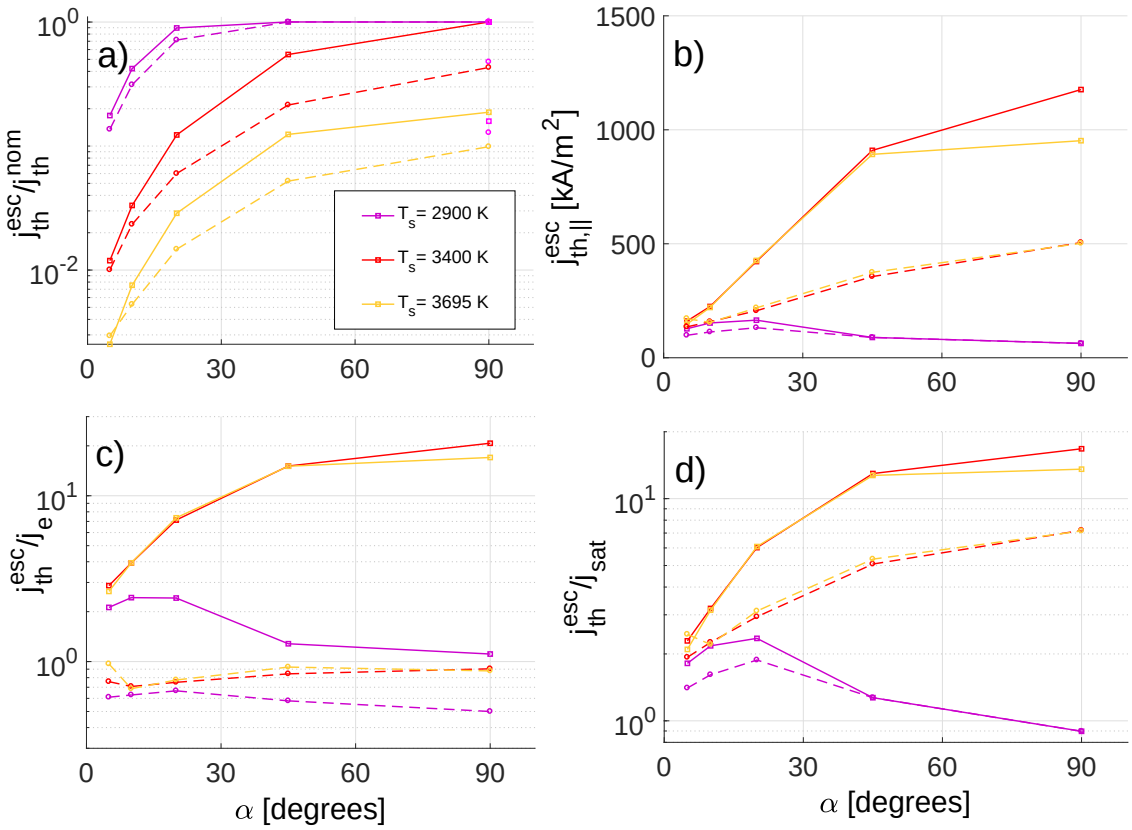

Figure 5. The escaping thermionic current $j_{\rm th}^{\rm esc}$ expressed (a) as a fraction of the nominal current given by the Richardson–Dushman formula, (b) as parallel current density in absolute units, (c) as a fraction of the incident electron flux, (d) as a fraction of the incident ion flux. Plots as a function of the inclination angle for different surface temperatures. The solid lines represent results for a fixed sheath potential drop and the dashed lines for a floating surface.

contribution of thermionic emission to the energy balance. In the fixed potential drop case; For $T_{\rm s} = 3400, 3695\,$K and near-normal inclination angles, the cooling flux is of the order or above 50% of the plasma heat flux, thus thermionic cooling of the surface is significant. However, for grazing incidence, this ratio drops towards $\sim 10\%$, as emission gets more severely suppressed - see Fig.5(a). In the floating case; Regardless of the inclination angle and the surface temperature, the cooling flux remains below 10% of the plasma heat flux. This is mainly due to the fact that the incident heat flux significantly increases due to the shift of the floating potential towards more positive values - see Fig.4(b).

Fig.6(b) depicts the total heat flux received by the PFC normalized by the total plasma heat flux incident to a non-emitting ($T_{\rm s} = 0\,$K) surface. Such an alternative representation allows us to determine whether thermionic emission needs to be considered in the total energy balance and the sheath heat transmission coefficient. Within the floating condition, thermionic emission indirectly leads to heating by increasing the plasma heat fluxes due to the positive shift in the floating potential which overcomes the direct cooling effect. This is a well known phenomenon from the literature of dust dynamics in fusion devices [42, 43]. Within the fixed

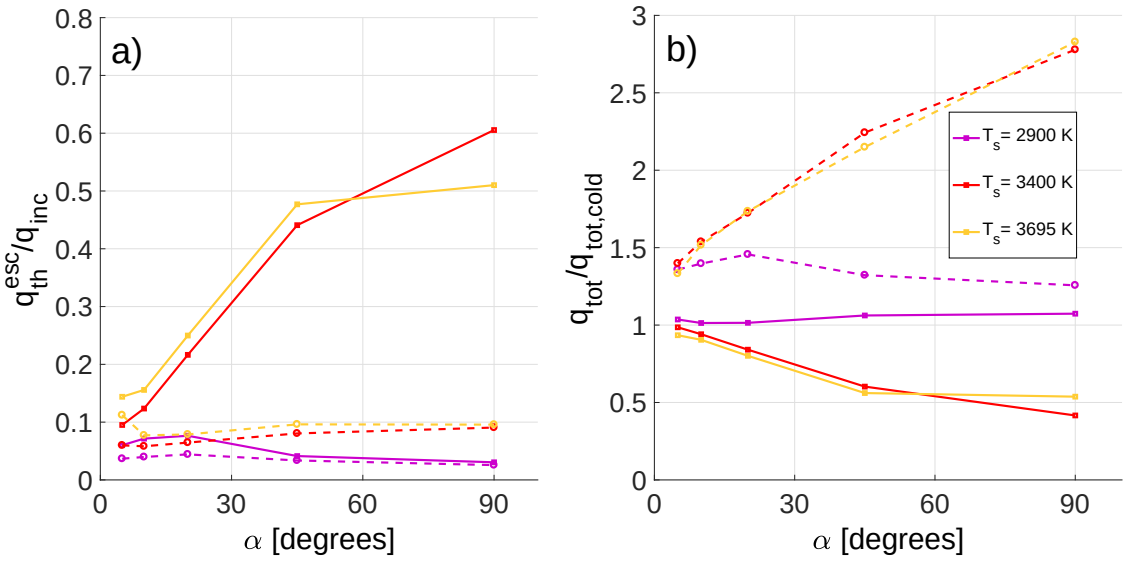

Figure 6. (a) The cooling flux to the PFC due to the escaping thermionic electrons $q_{\mathrm{th}}^{\mathrm{esc}}$ expressed as a fraction of the incident plasma heat fluxes q_{inc}. (b) The total heat flux q_{tot} received by the PFC normalized by the incident plasma heat fluxes q_{inc} for a non-emitting surface ($T_{\mathrm{s}} = 0\,\mathrm{K}$). Plots as a function of the inclination angle for different surface temperatures. The solid lines represent results for a fixed sheath potential drop and the dashed lines for a floating surface.

potential drop condition, thermionic emission only leads to direct cooling since the depth of the virtual cathode is negligible in T_{e}/e units leaving the plasma heat fluxes essentially unaffected. It is worth emphasizing that for grazing incidence in the fixed potential drop condition, regardless of the surface temperature, the total heat flux is nearly the same as in the non-emitting case, which is a clear consequence of the strongly suppressed emission.

3.2. Results for intra-ELM plasma conditions

During ELMs, the plasma species temperature $T_{\mathrm{e}} = T_{\mathrm{i}}$ is several times higher than during inter-ELM periods. Regardless of the magnetic field inclination angle, the sheath thickness will approximately scale as $h \propto (r_{\mathrm{L,i}}, \lambda_{\mathrm{D}}) \propto \sqrt{T_{\mathrm{e}}}$ and thus the normal electric field at the PFC surface will scale as $E_{\mathrm{n}}^{\mathrm{s}} \sim \phi_{\mathrm{s}}/h \propto \sqrt{T_{\mathrm{e}}}$ for a monotonic profile, which results to a larger repelling field for the emitted electrons unless the virtual cathode appears. On the other hand, the plasma density is only moderately increased and thus the incident particle flux $\propto n\sqrt{T}$ is not dramatically modified, which implies that the emission strength at $T_{\mathrm{s}} = 3695\,\mathrm{K}$ can be expected to suffice for the sheath to enter the space-charge limited regime. The results of the PIC simulations for selected scenarios (see subsection 2.3) are summarized in Table 1.

The results follow the same trends as for inter-ELM plasmas. Except for the case of normal inclination within the fixed wall condition, the virtual cathode is present and its magnitude increases for shallower angles. As far as the cathode depth and the sheath potential drop are concerned, the results are close to the inter-ELM scenario even quantitatively; the

Table 1. PIC simulations for $T_\mathrm{s} = 3695\,\mathrm{K}$ and plasma parameters relevant to JET Type I ELMs, *i.e.* $n_\mathrm{e} = 2\times10^{19}\,\mathrm{m}^{-3}$ and $T_\mathrm{e} = T_\mathrm{i} = 100\,\mathrm{eV}$. Results for varying inclination angles and different sheath potential drop assumptions.

Sheath drop	α	$\Phi_\mathrm{vc}\,[kT_\mathrm{s}/e]$	$\Phi_\mathrm{fl}\,[T_\mathrm{e}/e]$	$\eta_\mathrm{th} = j_\mathrm{th}^\mathrm{esc}/j_\mathrm{th}^\mathrm{nom}$	$j_{\mathrm{th},\|\|}^\mathrm{esc}$ [kA/m^2]	$q_\mathrm{th}^\mathrm{esc}/q_\mathrm{inc}$
Fixed	90°	0.0	-3.00	1.0	5100	0.11
Fixed	17.5°	2.68	-3.00	0.09	440	0.03
Fixed	5.0°	3.74	-3.00	0.006	31	0.01
Floating	90°	0.96	-0.84	0.38	2017	0.02
Floating	17.5°	3.00	-1.65	0.04	223	0.01
Floating	5.0°	3.78	-2.15	0.005	27	0.006

values presented in Fig.4(a) and (b) are within $10-15\%$ of those presented in Table 1. The escaping emitted current is still strongly inhibited but the suppression factor is few-to-several times larger compared to the inter-ELM results shown in Fig.5(a). As expected, PFC cooling due to thermionic emission is negligible compared to the heat impacted by the ELM plasma fluxes, since the heat fluxes scale as $nT^{3/2}$.

3.3. Comparison with theoretical models

Let us initially discuss the space-charge limited regime in the un-magnetized limit. The first analytical treatment of the problem in connection to the heat flow through the sheath has been carried out by Hobbs and Wesson [10]. The case of a floating surface, mono-energetic collisionless ions and zero temperature emitted electrons was studied. The analysis of the Poisson equation allowed the determination of algebraic conditions for the emergence of the non-monotonic potential which restricts the emission current to a value slightly below the incident electron current (we shall refer to this ratio as critical yield σ_e). Under the same assumptions for the ions, this treatment has been extended by Takamura and collaborators [12] for arbitrarily biased surfaces and finite emitted electron temperatures.

The normal incidence results can be compared with these models. For the floating surface under inter-ELM plasma conditions, from Fig.5(c) it can be observed that, for $T_\mathrm{s} = 2900\,\mathrm{K}$, the emission is not strong enough for the virtual cathode to form. However, once the surface temperature is high enough, the limit of the critical yield is reached, $\sigma_\mathrm{e} = 1 - 8.3\sqrt{m_\mathrm{e}/m_\mathrm{i}}$, which is 0.86 for deuterium ions - in accordance with the simulation values for $T_\mathrm{s} = 3400\,\mathrm{K}$ and $3695\,\mathrm{K}$. For the floating surface under intra-ELM plasma conditions, the simulation result is $\sigma_\mathrm{e} = 0.88$ which is also very close to the theoretical one. The Hobbs and Wesson model also predicts that the floating potential assumes the limiting value of $-1.02T_\mathrm{e}/e$, while the simulations lead to $-0.75T_\mathrm{e}/e$ for inter-ELM, see Fig.4(b), and $-0.85T_\mathrm{e}/e$ for intra-ELM, see Table 1, conditions. The discrepancy is within the accuracy level of these runs, briefly discussed in section 2.

For the biased surface, the Takamura model [12] provides a straightforward estimate of the escaping thermionic current in terms of the incoming ion flux (ion saturation) in the limit

of zero emitted electron temperature. For intra-ELM plasma conditions no virtual cathode was formed at normal incidence, thus only the inter-ELM results presented in Fig.5(d) can be employed for comparison. In particular, comparison is carried out with the results presented in Fig.3 of Ref.[12] for the bias of $-3T_e/e$. The latter yields $33j_{\rm sat}$ where $j_{\rm sat} = en_0\sqrt{T_{\rm e}/m_{\rm i}}$. For $T_{\rm s} = 3695\,{\rm K}$, our PIC simulations lead to $13j_{\rm sat}$ where $j_{\rm sat} = en_0\sqrt{(T_{\rm e}+T_{\rm i})/m_{\rm i}}$ which corresponds to $18j_{\rm sat}$ in the Takamura normalization. The source of such a discrepancy is currently under investigation.

It is important to emphasize that, for normal magnetic fields and independent of the sheath potential drop condition, the escaping current density should obey the relation $j_{\rm th}^{\rm esc} = j_{\rm th}^{\rm nom}\exp\left(-e\Phi_{\rm vc}/kT_{\rm s}\right)$ as a consequence of the Maxwellian distribution of the thermionic electrons and of the conservative nature of the repelling electrostatic potential. Substituting for the Richardson–Dushman formula, we end up with $j_{\rm th}^{\rm esc} = A_{\rm eff}T_{\rm s}^2\exp\left[-(W_{\rm f}+e\Phi_{\rm vc})/kT_{\rm s}\right]$, which implies that the virtual cathode effectively increases the material's work function. With the values provided in Fig.4(a) for the inter-ELM cases, we can calculate the escaping current density according to this expression and compare it with the PIC results, the computed values are illustrated by green circles in Fig.5(a). The deviations are within 15% in either direction, which is the limit of accuracy of the PIC results. For the floating case under ELM conditions, the computed result is 0.39 and coincides with the PIC ratio of 0.38 provided in Table 1.

We proceed with a brief discussion of prompt re-deposition. All analytical treatments of emission in the presence of oblique magnetic fields [15, 16] are based on the assumption of a monotonic potential profile and are thus valid for weak to moderate emission strengths. Under this assumption, the repelling electric field competes with return due to gyro-motion. On the other hand, in the presence of the virtual cathode, the emitted electrons are accelerated towards the surface, which also further enhances prompt re-deposition. Since the magnitude of the potential well is dictated by the escaping current, the effects of space-charge and prompt re-deposition are entangled and cannot be studied separately.

We shall compare our PIC results with the zero electric field limit of the Igitkhanov and Janeschitz model [16] in order to illustrate the importance of the inclusion of self-consistent electrostatic fields in the calculation of the emission suppression factor. The model provides the escaping current in terms of the space-charge limited current at 90° (see Fig.2 of Ref.[16] for $\beta = 0$). Since prompt re-deposition is most significant at shallow angles, we compare values for inclinations below 20°; For inter-ELM plasmas, the suppression factor provided by Ref.[16] is ~ 0.25, ~ 0.2 and ~ 0.1 versus the PIC results of ~ 0.15, ~ 0.05 and ~ 0.025 for 15°, 10° and 5°, respectively. For intra-ELM plasmas, the suppression factor provided by Ref.[16] is ~ 0.3, ~ 0.1 versus the PIC results of ~ 0.13, ~ 0.016 for 17.5° and 5°, respectively. To sum up, the inclusion of self-consistent electrostatic fields leads to a reduction of the suppression factor compared to pure gyro-return that is larger than a factor of four for nearly grazing incidence.

4. Summary and conclusions

The electrostatic sheath and magnetic pre-sheath of thermionically emitting planar tungsten surfaces has been simulated with the 2D3V SPICE2 PIC code with emphasis put on the thermionic suppression factor due to space-charge and Larmor gyration effects as well as on certain aspects of energy exchange with the surface. The fusion plasma conditions assumed are relevant for inter-ELM periods ($T_\mathrm{i} = T_\mathrm{e} = 20\,\mathrm{eV}$, $n_\mathrm{e} = 10^{19}\,\mathrm{m}^{-3}$, $B = 3\,\mathrm{T}$, deuterium plasma) but also for intra-ELM periods ($T_\mathrm{e} = T_\mathrm{i} = 100\,\mathrm{eV}$, $n_\mathrm{e} = 2 \times 10^{19}\,\mathrm{m}^{-3}$). Two boundary conditions have been considered; fixed sheath potential drop which implies no response from the plasma to the injected thermionic current, floating surface potential which implies a full plasma response. In many experiments, the actual situation might correspond to an intermediate plasma response between these two diametrically opposite limits, hence the applicability of the results has to be judged for individual experiments.

Fixed sheath potential drop. For normal magnetic field inclination and for the surface temperatures investigated here ($T_\mathrm{s} \leq T_\mathrm{melt,W} = 3695\,\mathrm{K}$), the virtual cathode forms only under inter-ELM conditions and at melting point temperatures. This implies that under intra-ELM conditions the thermionic current is totally unimpeded at least up to $T_\mathrm{s} = 3695\,\mathrm{K}$. As the inclination angle becomes more shallow, the thermionic suppression factor $\eta_\mathrm{th} = j_\mathrm{th}^\mathrm{esc}/j_\mathrm{th}^\mathrm{nom}$ rapidly decreases, since prompt re-deposition becomes more effective. Under inter-ELM plasma conditions and $T_\mathrm{s} = 3400\,\mathrm{K}$, the PIC results are $\eta_\mathrm{th} = 1,\ 0.1,\ 0.01$ for $\alpha = 90,\ 20,\ 5°$. On the other hand, at the melting point we have $\eta_\mathrm{th} = 0.2,\ 0.03,\ 0.001$ in the inter-ELM case and $\eta_\mathrm{th} = 1,\ 0.4,\ 0.006$ in the intra-ELM case for $\alpha = 90,\ 20\,(17.5),\ 5°$, respectively. As a result of the suppression, in the inter-ELM case, the surface cooling flux due to thermionic emission is comparable to the incoming heat flux at near-normal angles but this ratio is drastically reduced up to $10-15\%$ for grazing angles. On the other hand, for the limited intra-ELM scenarios investigated, this ratio decays from 10% to 1% for normal to $5°$ inclination. It is also worth pointing out that owing to $T_\mathrm{e} \gg kT_\mathrm{s}$ and $\Phi_\mathrm{vc} \sim kT_\mathrm{s}/e$, the incident plasma heat fluxes are not affected by the potential well.

Floating surface potential. Simulations have revealed that for normal magnetic field inclination the potential well can be formed for lower temperatures than in the fixed potential condition. The thermionic suppression factor η_th strongly decreases for grazing angles in the same manner as above. Under inter-ELM plasma conditions and $T_\mathrm{s} = 3400\,\mathrm{K}$, the results are $\eta_\mathrm{th} = 0.4,\ 0.05,\ 0.01$ for $\alpha = 90,\ 20,\ 5°$. On the other hand, at the melting point we have $\eta_\mathrm{th} = 0.1,\ 0.015,\ 0.01$ in the inter-ELM case and $\eta_\mathrm{th} = 0.4,\ 0.04,\ 0.005$ in the intra-ELM case for $\alpha = 90,\ 20\,(17.5),\ 5°$, respectively. In contrast to the depth of the potential well that is $\sim kT_\mathrm{s}/e$, the positive shift of the floating potential in the presence of emission is $\sim T_\mathrm{e}/e$. This implies a drastic increase in the incoming electron particle and heat flux, which masks cooling due to electron evaporation. Consequently, under this boundary condition, thermionic emission leads to significant indirect heating of the surface.

Future work will focus on the determination of the thermionic suppression factor for geometries (leading edge and sloped design) and plasma conditions (inter- and intra-ELM) relevant for repetitive transient tungsten melting experiments recently carried out in ASDEX

Upgrade [4]. The suppression factor constitutes an important input to melt-layer motion simulations of the macroscopic erosion profile [5,6] that will be compared to the post-mortem surface topography. Concerning modelling updates, the long term goal is to study the effect of spatial temperature gradients and realistic three dimensional geometries on thermionic current suppression but also to include electron induced electron emission, which is expected to be important for intra-ELM plasmas with $T_\mathrm{e} \geq 300$ eV.

Acknowledgments

The authors would like to thank Prof. Shuichi Takamura for useful information concerning details of his model. This work was supported by the Czech Science Foundation project GA16-14228S and co-funded by MEYS project number 8D15001. The simulations reported here have been performed at the National Computational Center IT4Innovations and the International Fusion Energy Research Centre cluster HELIOS. This work has also been carried out within the framework of the EUROfusion Consortium (WP PFC) and has received funding from the Euratom research and training programme 20142018 under grant agreement No 633053. The views and opinions expressed herein do not necessarily reflect those of the European Commission. S. R. and P. T would also like to acknowledge the financial support of the Swedish Research Council.

[1] Pitts R A, Bardin S, Bazylev B *et al.* accepted for publication in Nucl. Mat. Energy
[2] Coenen J W, Arnoux G, Bazylev B *et al.* 2015 *Nucl. Fusion* **55** 023010
[3] Coenen J W, Arnoux G, Bazylev B *et al.* 2015 *J. Nucl. Mater.* **463** 78
[4] Krieger K *et al.* submitted for publication to Nucl. Fusion
[5] Bazylev B, Janeschitz G, Landman I *et al.* 2009 *J. Nucl. Mater.* **390-391** 810
[6] Bazylev B *et al.* this issue
[7] Robertson S 2013 *Plasma Phys. Control. Fusion* **55** 093001
[8] Mizoshita S, Shiraishi K, Ohno N and Takamura S 1995 *J. Nucl. Mater.* **220-222** 488
[9] Takamura S, Mizoshita S and Ohno N 1996 *Phys. Plasmas* **3** 4310
[10] Hobbs G D and Wesson J A 1967 *Plasma Phys.* **9** 85
[11] Porter G D 1982 *Nucl. Fusion* **22** 1279
[12] Takamura S, Ohno N, Ye M Y and Kuwabara T 2004 *Contrib. Plasma Phys.* **44** 126
[13] Delzanno G L and Tang X-Z 2014 *Phys. Rev. Lett.* **113** 035002
[14] Tsvetkov I V and Tanabe T 1998 *J. Nucl. Mater.* **258-263** 927
[15] Tskhakaya D and Kuhn S 2000 *Contrib. Plasma Phys.* **40** 484
[16] Igitkhanov Yu and Janeschitz G 2001 *J. Nucl. Mater.* **290-293** 99
[17] Komm M, Dejarnac R, Gunn J P and Pekarek Z 2013 *Plasma Phys. Control. Fusion* **55** 025006
[18] Dejarnac R and Gunn J P 2007 *J. Nucl. Mater.* **363-365** 560
[19] Komm M, Dejarnac R, Gunn J P, Kirschner A, Litnovsky A, Matveev D and Pekarek Z 2011 *Plasma Phys. Control. Fusion* **53** 115004
[20] Herring C and Nichols M H 1949 *Rev. Mod. Phys.* **21** 185
[21] Modinos A 1984 *Field, Thermionic and Secondary Electron Emission Spectroscopy* (New York: Plenum Press)
[22] Michaelson H B 1977 *J. Appl. Phys.* **48** 4729
[23] Fomenko V S 1966 *Handbook of Thermionic Properties: Electronic Work Functions and Richardson Constants of Elements and Compounds* (New York: Plenum Press)
[24] Nottingham W B 1941 *Phys. Rev.* **59** 906
[25] Eckstein W and Biersack J P 1985 *Appl. Phys. A* **38** 123

[26] Cuthbertson J W, Langer W D and Motley R W 1992 *J. Nucl. Mater.* **196-198** 113
[27] Souda R, Aizawa T, Hayami W, Otani S and Ishizawa Y 1990 *Phys. Rev. B* **42** 7761
[28] Eckstein W 2009 Reflection (Backscattering) Technical Report IPP 17/12 Max Planck Institute for Plasma Physics
[29] Kozyrev A V and Shishkov A N 2002 *Tech. Phys. Lett.* **28** 504
[30] Gunn J P 2005 *J. Nucl. Mater.* **337-339** 310
[31] Harbour P J, Summers D D R, Clement S *et al.* 1989 *J. Nucl. Mater.* **162-164** 236
[32] Takahashi H, Fredrickson E D, Schaffer M J, Austin M E, Evans T E, Lao L L and Watkins J G 2004 *Nucl. Fusion* **44** 1075
[33] Pitts R A, Alberti S, Blanchard P, Horacek J, Reimerdes H and Stangeby P C 2003 *Nucl. Fusion* **43** 1145
[34] Faudot E, Heuraux S, Kubic M, Gunn J and Colas L 2013 *Phys. Plasmas* **20** 043514
[35] Tolias P 2014 *Plasma Phys. Control. Fusion* **56** 123002
[36] Tolias P 2016 arXiv:1601.02047v1
[37] Dejarnac R, Podolnik A, Komm M, Arnoux G, Coenen J W, Devaux S *et al.* 2014 *Nucl. Fusion* **54** 123011
[38] Birdsall C K and Langdon A B 1991 *Plasma Physics via Computer Simulation* (Bristol: Adam Hilger)
[39] Hakola A, Karhunen J, Koivuranta S, Likonen J, Balden M, Herrmann A *et al.* 2014 *Phys. Scr.* **T159** 014027
[40] Eich T *et al.* 2017 *Nucl. Fusion* (submitted)
[41] Delzanno G L, Camporeale E, Moulton J D, Borovsky J E, MacDonald E A and Thomsen M F 2013 *IEEE Trans. Plasma Sci.* **41** 3577
[42] Krasheninnikov S, Smirnov R and Rudakov D 2011 *Plasma Phys. Control. Fusion* **53** 083001
[43] Vignitchouk L, Tolias P and Ratynskaia S 2014 *Plasma Phys. Control. Fusion* **56** 095005